Communication and collective consensus making in animal groups via mechanical interactions

Péter L. Várkonyi[1]

The final version of the article is available at

http://www.springer.com/mathematics/analysis/journal/332

Mechanical constraints have strong influence on the dynamics, and structure of granular aggregations. The contact forces within dense suspensions of active particles may give rise to intriguing phenomena including anomalous density fluctuations, long-range orientational ordering, and spontaneous pattern formation. Various authors have proposed that these physical phenomena contribute to the ability of animal groups to move coherently. Our systematic numerical simulations confirm that spontaneous interactions of elongated individuals can trigger oriented motion in small groups. They are however insufficient in bigger ones, despite their significant imprint on the group's internal structure. It is also demonstrated that preferred directions of motion of a minority of group members can be communicated to others solely by mechanical interactions. These findings strengthen the link between pattern formation in active nematics, and the collective decision making of social animals.

[1] Budapest University of Technology and Economics, and California Institute of Technology; email: vpeter@mit.bme.hu

short title: Communication in groups via mechanical interactions

1. Introduction

Understanding the mechanisms operating in bird flocks, fish schools and other animal groups lacking leaders has received widespread attention in both physics, and biology [1]. Methods of statistical physics have been successfully applied to explore the macroscopic dynamics, and phase transitions of groups [2,3] initiated by local interactions of individuals. Among the rich variety of microscopic rules generating flocking, the most important are *attraction* (i.e. motion towards other individuals), and *alignment* (mimicking the heading of others) [4-7], which are considered as the two basic ingredients of oriented group motion.

Local interactions as simple as passive contact forces can lead to long-range or quasi-long-range ordering in particle sets, together with other peculiar phenomena such as anomalous density fluctuations and large-scale patterns. Liquid crystals, as well as actively moving or vibrated, apolar particles may exhibit nematic order [8-11]; polar grains with elongated [12-18] or even round [19-21] shapes also show polar ordering. Both types of ordering has been observed for biofilaments driven by molecular motors [22-24] and in aggregates of mobile bacteria, whose interaction includes hydrodynamic coupling [25,26], and perhaps contact forces [18]. Based on the analogy between (polarly oriented) clusters of physical particles, and (oriented motion of) groups, many authors have suggested that passive mechanical interactions help various biological agents to gather into swarms, as well as to move coherently, see e.g. [7,10,18]. There is sufficient evidence for the first part of this statement, however the second part has only been investigated in dense aggregates of many particles moving in finite space, typically with periodic boundaries, representing a finite sample from a quasi-infinite set. In these models, nothing (but perhaps some explicit noise) works against

ordering, and some works even reported global orientational order regardless of the number of interacting particles [19,21]. The aim of the current paper is to examine a more realistic setting, in which the ordering mechanism rivals other effects such as cohesion. We study isolated, finite-sized groups, which stay together via active social interactions, but rely solely on passive interactions to achieve and maintain a common direction of motion. In addition to spontaneous, oriented group motion, it is also examined how the preferred heading of an informed (but unidentified) minority in the group is 'communicated' to the rest of the group by contact forces. The ecological significance of both tasks is straightforward: the former allows members to enjoy the advantages of staying together, and simultaneously to travel large distances while exploring limited resources (e.g. food or water). The latter is a toy model of escaping from predators, or guiding group members towards a newly discovered food source. It has been shown that these tasks are efficiently solved by groups, in which individuals monitor the heading of their close neighbors, and align themselves; the best quality of synchronization is achieved by big groups due to the averaging out of disturbances [27,28]. Our main finding (Section 3) is that the elementary mechanical interactions can almost perfectly substitute social alignment as long as the group in question is sufficiently small, and individuals have elongated shapes. The efficiency of the mechanism however breaks down as group size is increased.

In our model (Section 2), individuals are represented by self-propelled, planar, rigid bodies moving in unbounded two-dimensional space, and exhibiting hard, frictionless collisions. To maintain group cohesion, a simple form of distance-independent all-to-all *attraction* is assumed among individuals. *Alignment* is not included explicitly in the model; this distinction between the two forms of social behavior is biologically relevant since alignment requires sensing the directions of motion of other individuals, which is a much more complex task than

tracking their positions. The simulation of the continuous dynamics combined with hard impacts is based on a custom-made variational principle of rigid body mechanics.

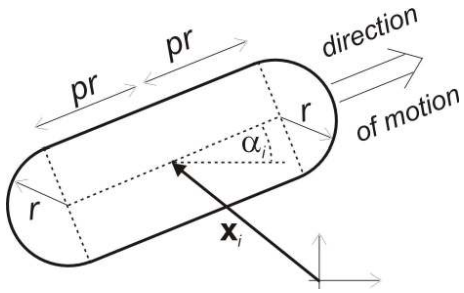

Figure 1: The shape of one particle

2. Description of the model

We consider n two dimensional self-propelled rigid objects, each of which consists of two semicircles of radius r, and a rectangle of size $2r \times 2pr$. The position of particle i is described by a vector $\mathbf{x}_i$ pointing to its centre, and an orientation angle α_i, which is defined as the angle between the forward pointing longitudinal axis of the particle and a fixed axis in a global frame (Figure 1). In the absence of body contacts, each particle moves forward by a constant speed, which is denoted by v_0. Hence, the velocity vector of the particle's centroid is

$$\dot{\mathbf{x}}_{i,unc} = v_0 \cdot \begin{bmatrix} \cos\alpha_i \\ \sin\alpha_i \end{bmatrix} \tag{1}$$

The index '$_{unc}$' of the velocity indicates that this equation holds while motion is not constrained by contacts. Simultaneously to translational motion, each individual turns towards its preferred direction represented by a vector $\mathbf{p}_i$. The associated angular velocity is

$$\dot{\alpha}_{i,unc} = \mathbf{p}_i^T \cdot \begin{bmatrix} -\sin\alpha_i \\ \cos\alpha_i \end{bmatrix} \tag{2}$$

where the dot operator represents scalar product, and ^{T} means transpose. The preference vector $\mathbf{p}_i$ is the weighted sum of two components:

$$\mathbf{p}_i = c_{p,i}\mathbf{p}_{p,i} + c_s\mathbf{p}_{s,i}. \quad (3)$$

The unit vectors $\mathbf{p}_{p,i}$ are the intrinsic directional preferences of the informed individuals, which reflect their knowledge about food sources, migration routes or dangerous locations. These vectors are kept fixed during the simulation. For uninformed individuals, $c_{p,i}$=0 hence $\mathbf{p}_{p,i}$ has no role. The second term implements social attraction to other individuals. $\mathbf{p}_{s,i}$ is calculated as

$$\mathbf{p}_{s,i} = \frac{1}{n-1}\sum_{j\neq i}\frac{\mathbf{x}_j - \mathbf{x}_i}{\left|\mathbf{x}_j - \mathbf{x}_i\right|}. \quad (4)$$

i.e. it is a vector of length between 0 and 1, pointing towards the 'center of mass' of the n individuals. The proposed form of distance-independent all-to-all attraction is one of the standard ways of modeling social cohesion (e.g. [29]), but not necessarily the most realistic one [30]. Previous works have also used all-to all cohesion below a given distance threshold [27,31] (which often exceeds groups size and results in effectively all-to-all interaction), increasing [32] or decaying [33] functions of distance, or interactions with a limited number of close neighbors [7]. Our focus is on small groups, in which the distance between the individuals is also limited, and thus all alternatives are practically similar. In the context of the present model, interactions limited to immediate neighbors in terms of a Voronoi diagram (as in [7]) was also tested, and this rule yielded similar results to (4).

Next we give a brief summary of the simulation of the full system including volume exclusion constraints. For a more comprehensive description, the reader is advised to consult the Appendix. Equations (1),(2) can be interpreted as the overdamped motion of an object driven by propulsive forces and torques in the presence of Stokes drag in a viscous medium. The

damping coefficients for translational (ρ_1) and rotational (ρ_2) motion do not influence unconstrained motion, but they have some effect on constrained dynamics. The kinetic interpretation of the equations of motion allows to complement them by contact forces and impacts; these are however unknown. Instead of their direct calculation, we take a variational approach inspired by the classical Principle of Least Constraint (PLC) [34]. According to the PLC, the generalized acceleration of a constrained system is as close to the 'unconstrained acceleration' dictated by the free forces, as possible; in particular, if the unconstrained acceleration is consistent with the constraints, then it is adopted by the system. This principle is an efficient tool of rigid body simulations without friction, but it is not applicable to overdamped systems such as the present model. In the Appendix, we derive an analogous variational principle for overdamped systems, which also implements collisions, and is adapted to discrete-time simulations. Let the positions $\mathbf{x}_i(t), \alpha_i(t)$ of the objects be given at time *t*. Let equations (1),(2) predict $\dot{\mathbf{x}}_{i,unc}(t), \dot{\alpha}_{i,unc}(t)$ unconstrained velocities, and let

$$\mathbf{x}_{i,unc}(t+\Delta t) \overset{def}{=} \mathbf{x}_i(t) + \dot{\mathbf{x}}_{i,unc}(t) \cdot \Delta t \tag{5}$$

$$\alpha_{i,unc}(t+\Delta t) \overset{def}{=} \alpha_i(t) + \dot{\alpha}_{i,unc}(t) \cdot \Delta t \tag{6}$$

Then,

Principle 1: the updated configuration $\mathbf{x}_i(t+\Delta t), \alpha_i(t+\Delta t)$ *of the constrained system after a small time step* Δt *is the minimizer of the quadratic function*

$$\rho_1 \sum_{i=1}^{n} \left(\mathbf{x}_i(t+\Delta t) - \mathbf{x}_{i,unc}(t+\Delta t)\right)^2 + \rho_2 \sum_{i=1}^{n} \left(\alpha_i(t+\Delta t) - \alpha_{i,unc}(t+\Delta t)\right)^2 \tag{7}$$

among all values that satisfy the volume exclusion constraint (up to an $O(\Delta t^2)$ *error term).*

Principle 1 naturally lends itself to numerical integration of the full dynamics of the system. We perform simulations with up to approximately 10^2 individuals, which is sufficiently high to capture the transition from almost perfect order to effectively unordered motion. Details of the implementation are also found in the Appendix.

The model has 4 dimensionless parameters, which are listed in Table 1 together with the values used here. The most important one is π_1 controlling particle shape, which is systematically varied in the simulations between 1 and 8. π_2 is 0 in the first series of simulations where spontaneous motion of a group without intrinsic directional preferences is analyzed (Section 3.1). In a second series of simulations (Section 3.2), where such preferences are included, the value π_2=0.5 ensures that preferences of some group members may not overcome group cohesion and cause splitting. Parameter π_3 determines the maneouvrability of the individuals. Very high turning rates suppress oriented motion. On the other hand, very low turning rates result in loose groups, in which mechanical interactions rarely occur. Thus, the intermediate value π_3=1 is chosen, which also yields trajectories comparable to the real motion of various animals and bacteria. Finally, π_4 enters through *Principle 1*. High values of π_4 mean that contact forces turn objects easily rather than displacing their centroids. There seems to be no straightforward recipe for 'realistic' values of π_4 due to the abstract nature of the model and the wide range of physical interactions it may represent. The choice π_4=10 is based on visual inspection of simulated particle-particle interactions. To illustrate the effects of π_3 and π_4, and to support our choice, five short animations are attached [35].

Table 1: Dimensionless model parameters. Particle size *s* is defined as the arithmetic mean of body length and body width, i.e. $s=2r(1+p/2)$.

Parameter	Meaning	Value in 1st series	Value in 2nd series
$\pi_1 = 1 + p$	Length-width ratio of particle	Systematically varied between 1, and 8	
$\pi_2 = \frac{c_{p,i}}{c_s}$	Strength of intrinsic preference relative to social attraction	0	0.5 for informed, 0 for uninformed individuals
$\pi_3 = \frac{sc_s}{v_0}$	Ratio of body size s (defined in caption) to turning radius	1	
$\pi_4 = \frac{\rho_1}{\rho_2} s^2$	Sensitivity of drag force to velocity relative to that of drag torques to angular velocity. Fore more explanation, see the Appendix	10	

The current model does not include noise explicitly, even though it is inherently present in biological systems, and it strongly affects the dynamics in certain situations (see for example [36]). Most notably, some noise may enhance synchronization, and other types of ordering in some dynamical systems including swarms [16,37,38]. In our case, numerical experiments with added noise show typically similar dynamics with somewhat noisier results. This is not surprising, since the attraction forces of the model perturb oriented motion somewhat similarly to noise.

3. Results

3.1 Spontaneous motion

In these simulations (see also [39]), the individuals have no directional preferences (π_2=0), i.e. they are driven purely by social attraction. Simulation results with π_1=1, 2, 4, 8, and with various values of n between 3 and 74 are reported. For each combination of the parameter values, several runs are averaged, each of which covers a time interval of length $1000s/v_0$

(where *s* is particle size defined in the caption of Table 1). Before each run, the particles are assigned independent, uniformly distributed, random initial orientation angles (from the interval $(0,2\pi)$) and positions (within a disk of reasonable size depending on *n*). If two particles overlap, one of them is assigned a new initial configuration. Initial transient dynamics is typically only observable during a small portion of the simulations, thus the entire simulation is used for statistical evaluation.

The orientational order in the group is measured by the time average of the normalized speed of the group centroid, i.e.

$$v = \frac{1}{nv_0}\left\langle \left| \sum_{i=1}^{n} \dot{\mathbf{x}}_i \right| \right\rangle \tag{8}$$

where ||, and <> stand for Euclidean length, and time average, respectively. This quantity is always nonnegative, and it takes the maximum value 1 if every particle moves in the same direction. In case of an unordered group, the mean value of *v* is

$$v_{ind}(n) = A(n)/n \tag{9}$$

where $A(n)$ is the mean size of the sum of *n* randomly oriented unit vectors with uniform distribution. A closed formula for $A(n)$ can be found in [40,41]; $A(n)$ is approximately $n^{1/2}$, hence for big *n*, v_{ind} is almost 0.

The values of *v* measured in the simulations, as well as $v_{\mathrm{ind}}(n)$ are shown in Figure 2. The simulation results reveal dramatic difference between round, and elongated individuals. For $\pi_1=1$, the speed of the group centroid tends to be *under* the reference value $v_{\mathrm{ind}}(n)$, which indicates negative correlation of individual headings. This is not very surprising, given that the corresponding group structure resembles a solid crystal (Figure 3, right panel). This curve has an increasing portion if $n<10$ due to the fact that very small groups tend to follow periodic

patterns with very few or no contact among particles. The π_1=4 and 8 curves show almost perfect ordering for $n \leq 10$, and significant amount of orientational order throughout the tested range. They are close to one another, indicating that this degree of elongation is enough to fully provoke the ordering mechanism. As n is increased, the nematic order of the group is gradually destabilized by individuals travelling at the front of the cluster and willing to turn back in response to social attraction. This gives rise to a continuously changing dynamic internal group structure and fluctuations of the order parameter instead of a stable ordered cluster.

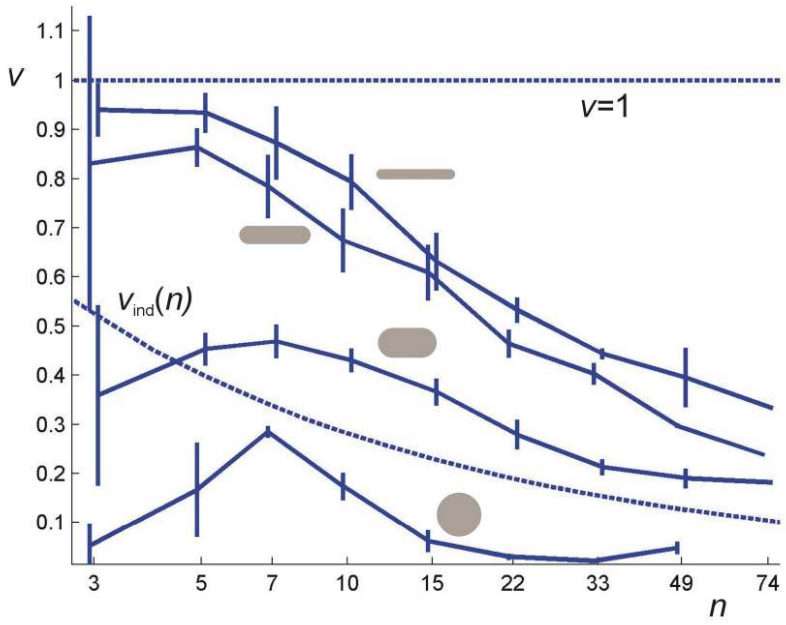

Figure 2: logarhythmic plot of the mean speed v of the group centroid as function of number n of individuals (solid lines). Error bars indicate standard deviation normalized by the number of runs minus 1. The four curves represent π_1=1, 2, 4 and 8. The corresponding body shapes are shown as grey contours. The dashed line near the bottom represents expected velocities v_{ind} in case of an unordered group.

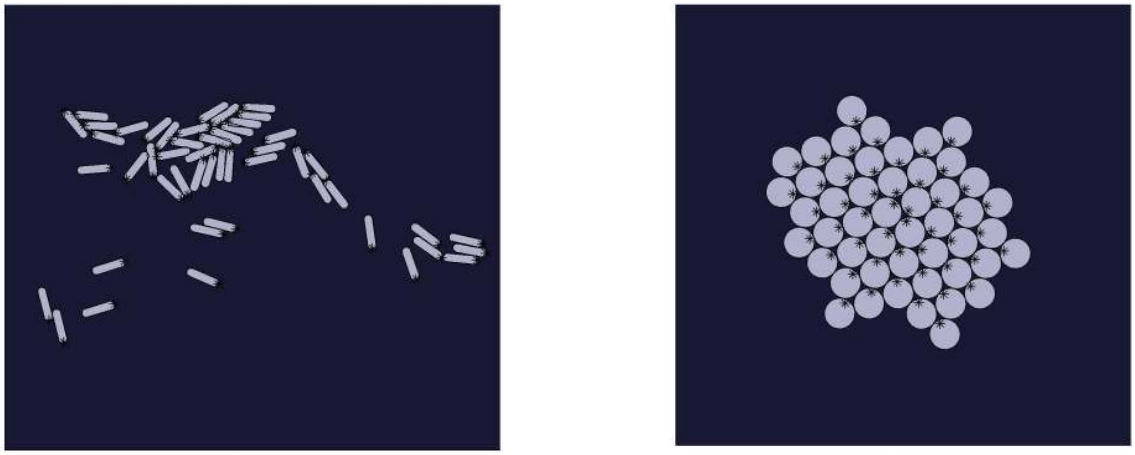

Figure 3: typical snapshots of a group, see also the animations [39]. The 'heads' of the individuals are marked by dark stars. Left: oriented clusters if π_1=4, n=50. Right: tightly packed group with no directional order if π_1=1, n=50. Other parameter values are specified in the text.

To gain some insight into the internal dynamics of a group (and into fluctuations of v), we introduce an a priori threshold v_{th} (=2/3) of v, above which the state of the group is considered as 'ordered'. From time to time, the group switches between the ordered and the unordered states. We define 'buildup' and 'breakdown' times as the average length of time intervals spent continuously in unordered, and ordered states, respectively. Measured values are shown in Figure 4. Buildup times increase exponentially with n; the mechanical interactions can very rarely bring groups into ordered state if n significantly exceeds 10 even if the particles are elongated. On the other hand, the breakdown times are still high above 1 if n=50 (provided that $\pi_1 \geq 4$), reflecting the fact, that these limited interactions are able to maintain the ordered state for a significant time, once it has been established. The two results together suggest that even though perfect orientational ordering requires more efficient mechanisms, mechanical interactions still have an important contribution to the maintenance of group order.

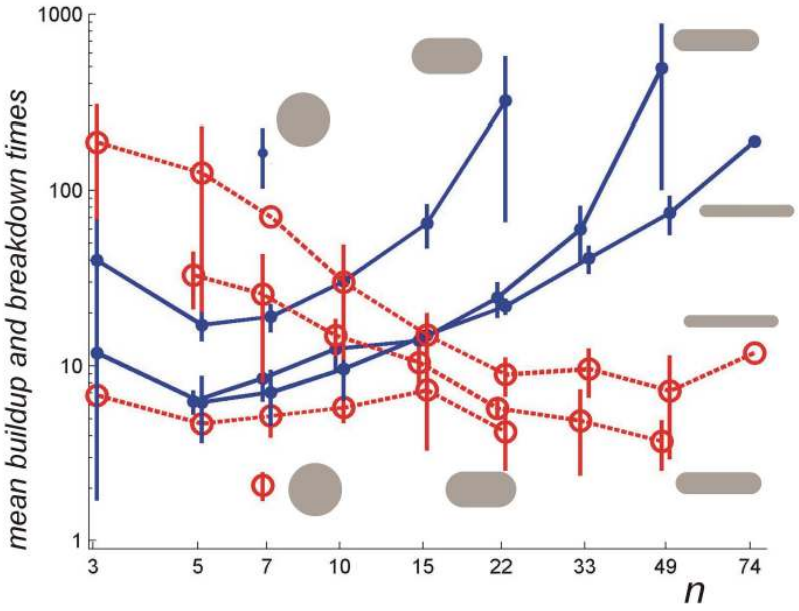

Figure 4: average buildup (filled circles) and breakdown (empty circles) times of the ordered state as functions of *n*. Notice the logarithmic scales. Data is shown only if the ordered state is reached at least once during every simulation with given set of parameter values.

The last thing to notice about the first series of simulations is that big groups of elongated particles hardly ever become fully ordered, nevertheless they show characteristic internal structure, in the form of continuously splitting and rebuilding smaller, oriented clusters (Figure 3, left panel). This appears to be analogous to the patterns observed in large sets of particles, which have been extensively studied elsewhere. The focus of this paper is not on these patterns, thus we only briefly mention a crude estimation of the average sizes of these clusters using v. For simplicity we assume that the group consists of n/n_{eff} oriented clusters, each of which is of equal size n_{eff}. If furthermore the orientations of different subgroups are independent of each other, than the mean speed of the group centroid becomes $v_{\mathrm{ind}}(n/n_{\mathrm{eff}})$. Hence n_{eff} can be estimated via interpolation from v, with help of the curve $v_{\mathrm{ind}}(n)$, cf. Figure 5. For $\pi_1 \geq 4$, n_{eff} is close to n for groups of consisting of only a few individuals (corresponding

35 to perfect ordering), and $n_{eff} \approx 10$ is obtained in case of n=50. The curves suggest that n_{eff}

36 probably saturates as n goes to infinity.

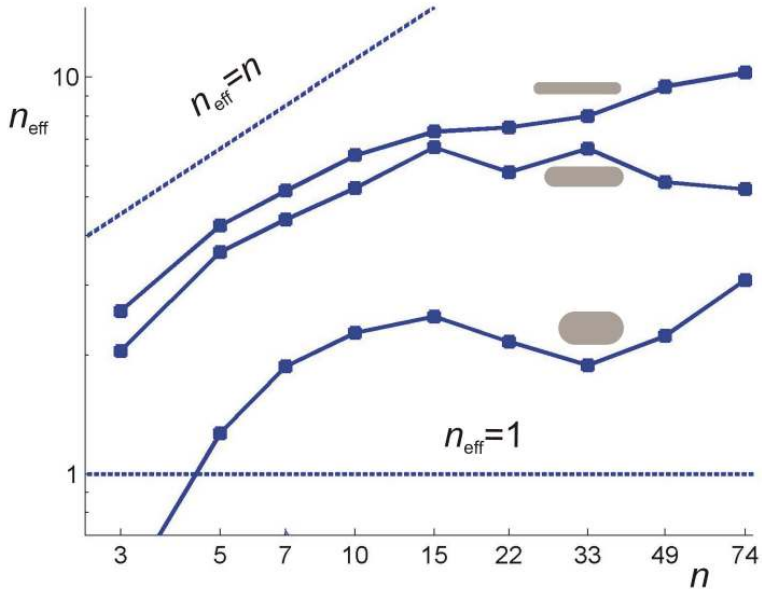

Figure 5: Effective size n_{eff} of ordered clusters as function of n.

3.2 Motion in a preferred direction

To test how information is transmitted in groups via contact forces, a second series of simulations was done, in which k individuals out of n had the same intrinsic preferred direction of motion (π_2=0.5), and the rest had no intrinsic preference (π_2=0). 16 runs for n=10,20 and 8 runs for n=40 of length 1000 time units (as defined in Section 3.1) were executed with each parameter combination (k,p) and the mean speed v_{pd} of drift in the preferred direction was measured in each case (Fig. 6). Other parameters and initial values were the same as in Section 3.1

The drift velocities clearly show that elongated body shape helps information propagation in the group, and increases the drift speed by up to a factor of 2. There is significant variation over different runs, especially with smaller groups size (n=10), and elongated shapes,

indicating that the group exhibits one of various stable structures depending on the initial conditions. It is also notable that moderately elongated individuals ($2 \leq \pi_1 \leq 4$) sometimes perform better than very elongated ones. This appears to be the consequence of very stable oriented clusters of uninformed individuals in the latter case, which are less efficiently driven by a small number of informed ones. Adding some noise or decreasing π_4 would change this counterintuitive trend.

If body shape is elongated and $n \leq 20$, the mean values for the velocity v_{pd} are significantly higher than the fraction k/n of informed group members, which means that even a minority of the group can efficiently guide the rest in a preferred direction. Couzin et al. [27] reported similar behavior in the context of more complex social interactions including social alignment. Hence, our simulations indicate that the efficiency of indirect communication via mechanical interactions of elongated objects is comparable to communication via direct alignment to nearby group members. There is however one major qualitative difference between the two cases: with social alignment, the fraction of informed individuals needed to guide the whole group in the right direction is lower in a big group than in a smaller one. In our case, comparison of results with n=40, and n=10-20 (cf. Fig. 6) suggests the opposite. This difference seems to reflect the extremely short range of mechanical interactions, leading to decreased efficiency in big aggregates.

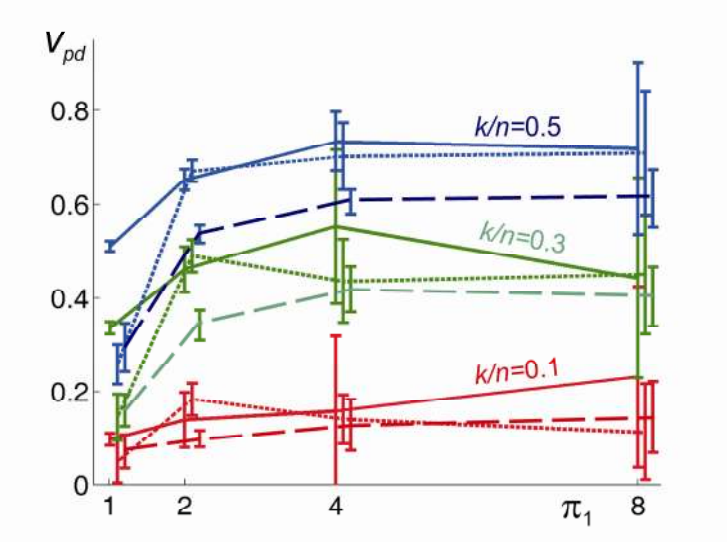

Figure 6: A: Mean drift speed of a group consisting of *n*=10 (solid lines), *n*=20 (dotted lines lines) and *n*=40 (dashed lines) individuals as a function of shape parameter π_1. Errorbars represent standard deviation for 16 (8 in the case *n*=40) runs. The fraction *k*/*n* of individuals with (identical) intrinsic directional **preferences is varied between 0.1, and 0.5.**

4 Discussion

The main finding of this paper is that mechanical interactions can lead to collective consensus making in *small groups* on the move, if the individuals' body shape is elongated. They are however insufficient to generate ordering in bigger ones. Indirect signaling of individual knowledge about optimal directions of motion was also found to be possible via contact forces. In this case, the short range of mechanical interactions counteracts the positive effect of noise averaging in big groups, and lower efficiency of communication was obtained for higher group sizes.

Small, orientationally ordered groups are very often formed by higher order animals such as equids, fish, certain insects, or birds [1], many of which are able to apply more complex social behavioral rules, including direct alignment to neighbors. For this reason, the most significant

message of this paper is that mechanical interactions contribute to the global ordering of groups, and their effects should be taken into account in studies of collective motion. In this respect, the mechanical ordering mechanism is less strictly limited to small groups: as we found in Section 3.1, the contact forces have strong contribution to the maintenance of existing ordered structures even in those groups, which are too big to be ordered solely by them.

Mechanical interactions are more important in tightly packed groups than in loose ones. It is remarkable that animal groups often become denser in emergency situations (e.g. in case of predator attack), thereby increasing the intensity of mechanical interactions as well. Our results suggest that this reaction may improve the group's chance of escaping such a dangerous situation; nevertheless it is beyond the scope of this paper to judge the evolutionary significance of this behavioral pattern.

Members of some animal groups do establish physical contact (e.g. sheep) as assumed in our model. In many real cases, individuals (e.g. birds) avoid collisions as part of their social interactions. The results of this paper are not directly applicable to the latter situation. However, hard, inelastic collisions represent a minimal-effort strategy of avoiding overlapping among rigid objects, according to a variational principle similar to the one used here [42]. This fact strongly suggests that hard interactions are analogous to economical collision avoidance schemes applied by biological agents, and that the latter have similar effects on orientational order.

5 Acknowledgements

I thank Günther Rote for his introduction to the Principle of Least Constraint, as well as Gábor Vásárhelyi, and Tamás Vicsek for their helpful comments. A part of this work was done while I enjoyed the hospitality of the Dept. of Mechanical Engineering at Caltech as a HAESF Senior Fellow. This work was also supported by the OTKA grant 72368 of the Hungarian Scientific Research Fund.

6 Appendix: the simulation of constrained dynamics

While the simulation of the differential equations (1)-(2) is straightforward, incorporating the hard interactions among particles is much more challenging, because contact forces are unknown, and impulsive interactions are also possible. As first step towards the complete model, (1)-(2) are approximated by Newtonian (force-acceleration) equations:

$$m\ddot{\mathbf{x}}_i = \rho_1\left(\dot{\mathbf{x}}_{i,unc} - \dot{\mathbf{x}}_i\right) \overset{def}{=} \mathbf{F}_{i,unc} \tag{10}$$

$$\theta\ddot{\alpha}_i = \rho_2\left(\dot{\alpha}_{i,unc} - \dot{\alpha}_i\right) \overset{def}{=} M_{i,unc} \tag{11}$$

where m, and θ are the masses, and the moments of inertia of the particles respectively. The right sides of the equations are the sums of the free forces ($\mathbf{F}_{i,unc}$), and torques ($M_{i,unc}$) acting on particle i. Each has two components, the first ones can be thought of as propulsive force, and torque, and the second terms are linear drag forces, and torques. The parameters ρ_i represent the intensities of each type of drag. The new equations predict the same dynamics as (1)-(2) in the limit $m,\theta\rightarrow 0$, which is referred to in the paper as overdamped limit.

It is theoretically possible to complement the right sides of equations (10),(11) with the constraint forces, and their torques, these are however unknown, and often ambiguous as long

as the individual objects are considered rigid. Instead of doing so, we derive a variational principle that can be used to simulate the system's behavior in the overdamped limit without calculating the constraint forces. The simplicity of the below presented results is due to the fact that we assumed the drag to be *linear function* of the velocities in (10),(11). The new principle is analogous to the classical Principle of Least Constraint (PLC) [34], however the PLC applies only for regular systems that are not in the overdamped limit.

D'Alembert's principle states that the virtual work of constraint forces in mechanical systems is always zero. In a two dimensional system of rigid bodies with identical masses (m), and inertias (θ), this means

$$\sum_{i=1}^{n}\left(\mathbf{F}_{i,unc}-m\ddot{\mathbf{x}}_i\right)\delta\mathbf{x}_i+\sum_{i=1}^{n}\left(M_{i,unc}-\theta\ddot{\alpha}_i\right)\delta\alpha_i=0 \tag{12}$$

for arbitrary virtual displacements (and rotations) $\delta\mathbf{x}_i$, $\delta\alpha_i$, which are consistent with the constraints. One way to obtain the above virtual displacements is by virtual variations of the particles' velocities during a small time interval τ, which also need to be in accord with the constraints. Substituting

$$\delta\mathbf{x}_i=\delta\dot{\mathbf{x}}_i\tau \tag{13}$$

$$\delta\alpha_i=\delta\dot{\alpha}_i\tau \tag{14}$$

into (12) yields

$$\sum_{i=1}^{n}\left(\mathbf{F}_{i,unc}-m\ddot{\mathbf{x}}_i\right)\delta\dot{\mathbf{x}}_i+\sum_{i=1}^{n}\left(M_{i,unc}-\theta\ddot{\alpha}_i\right)\delta\dot{\alpha}_i=0\,. \tag{15}$$

$\mathbf{F}_{i,unc}$, and $M_{i,unc}$ are given by the equations (10),(11) of unconstrained motion, thus

$$\sum_{i=1}^{n}\left(\rho_1\left(\dot{\mathbf{x}}_{i,unc}-\dot{\mathbf{x}}_i\right)-m\ddot{\mathbf{x}}_i\right)\delta\dot{\mathbf{x}}_i+\sum_{i=1}^{n}\left(\rho_2\left(\dot{\alpha}_{i,unc}-\dot{\alpha}_i\right)-\theta\ddot{\alpha}_i\right)\delta\dot{\alpha}_i=0 \tag{16}$$

The terms proportional to m or θ vanish in the overdamped limit, yielding

$$\rho_1 \sum_{i=1}^{n} \left(\dot{\mathbf{x}}_{i,unc} - \dot{\mathbf{x}}_i \right) \delta \dot{\mathbf{x}}_i + \rho_2 \sum_{i=1}^{n} \left(\dot{\alpha}_{i,unc} - \dot{\alpha}_i \right) \delta \dot{\alpha}_i = 0 \tag{17}$$

This expression can be rewritten as

$$-\frac{\rho_1}{2} \sum_{i=1}^{n} \delta \left(\dot{\mathbf{x}}_{i,unc} - \dot{\mathbf{x}}_i \right)^2 - \frac{\rho_2}{2} \sum_{i=1}^{n} \delta \left(\dot{\alpha}_{i,unc} - \dot{\alpha}_i \right)^2 = 0 . \tag{18}$$

i.e. the left hand side is the variation of a single quadratic function:

$$\delta \left[\rho_1 \sum_{i=1}^{n} \left(\dot{\mathbf{x}}_{i,unc} - \dot{\mathbf{x}}_i \right)^2 + \rho_2 \sum_{i=1}^{n} \left(\dot{\alpha}_{i,unc} - \dot{\alpha}_i \right)^2 \right] = 0 . \tag{19}$$

This function represents the deviation of the real velocities of the constrained system from the values it would have in the absence of constraints (cf. (1),(2)). This quantity is stationary by (19). In fact, the deviation is always *minimized* by the actual values of $\dot{\mathbf{x}}_i$, and $\dot{\alpha}_i$. Thus, the unknown velocities, and angular velocities of the objects can be obtained by minimizing a quadratic objective function.

A first approach to simulations with the help of equation (19) is the following:

1. From the positions ($\mathbf{x}_i$, α_i) of the objects, one can determine the unconstrained velocities ($\dot{\mathbf{x}}_{i,unc}$, $\dot{\alpha}_{i,unc}$) using (1),(2).
2. The positions also allow to determine the actual constraints of the motion, which depend on the shapes (π_1) and the sizes (r) of the individuals. In terms of velocities, the constraint is the following: if the distance between the closest points of two objects is positive, then they may have arbitrary velocities. If the distance is 0, then the time derivative of the distance is nonnegative. The latter condition yields linear inequalities for the velocities $\dot{\mathbf{x}}_i$, $\dot{\alpha}_i$.
3. Given the results of the first two steps, the constrained optimization problem (19) is solved for ($\dot{\mathbf{x}}_i$, $\dot{\alpha}_i$).

4. Next, a small time steps of size Δt is considered, during which the objects are assumed to have constant velocities. Hence, the positions are updated according to

$$\mathbf{x}_i(t+\Delta t) = \mathbf{x}_i(t) + \Delta t \cdot \dot{\mathbf{x}}_i(t) \tag{20}$$

$$\alpha_i(t+\Delta t) = \alpha_i(t) + \Delta t \cdot \dot{\alpha}_i(t) \tag{21}$$

5. From this point, the whole cycle is repeated with updated positions

The drawback of this method is that small numerical errors in velocities can accumulate over many time-steps to produce a macroscopic error in the positions, and overlapping objects. This shortcoming can be eliminated by noticing that the minimal deviation of the actual velocities $\dot{\mathbf{x}}_i, \dot{\alpha}_i$ from the 'unconstrained' values $\dot{\mathbf{x}}_{i,unc}, \dot{\alpha}_{i,unc}$ implies, that after a small time step, the deviation of the updated positions $\mathbf{x}_i(t+\Delta t), \alpha_i(t+\Delta t)$ from the hypothetical values $\mathbf{x}_{i,unc}(t+\Delta t), \alpha_{i,unc}(t+\Delta t)$ is also minimal (cf. equations (5),(6),(20),(21)). Thus, the variational principle (19) is equivalent of *Principle 1*, which is stated in Section 2.

The simulations of this paper are based on *Principle 1*. One time-step of the applied simulation method consists of the following parts:

1) determination of $\dot{\mathbf{x}}_{i,unc}$, and $\dot{\alpha}_{i,unc}$ using (1), (2), and the actual positions of the particles
2) determination of $\mathbf{x}_{i,unc}(t+\Delta t)$, and $\alpha_{i,unc}(t+\Delta t)$ from (5),(6).
3) determinations of the constraints in terms of *positions*. The condition is that the two objects should not overlap. This yields nonlinear inequalities for $\mathbf{x}_i(t+\Delta t)$, $\alpha_i(t+\Delta t)$, which can be linearized about the point $\mathbf{x}_i(t), \alpha_i(t)$ to obtain linear constraints.
4) Application of *Principle 1* to find $\mathbf{x}_i(t+\Delta t), \alpha_i(t+\Delta t)$

The bulk of the computational capacity is needed to obtain the last step, which requires the minimization of a quadratic function under linear inequality constraints, i.e. a *standard quadratic programming problem*. There are numerous algorithms for this, nevertheless its complexity yields an upper bound on the number of simultaneously interacting objects. The author's Matlab-based implementation of this algorithm was able to handle a group of approximately 120 individuals on a standard Pentium 4 PC. The time needed to perform a simulation depends strongly on the size of the swarm. For few individuals, simulations similar to the attached movie [39] can be done real-time. For 100 individuals, the simulation process is approximately two orders of magnitude slower.

References

[1] Sumpter, D. J. T., *Collective Animal Behavior*, Princeton University Press, Princeton (2009). Available online at http://www.collective-behavior.com/

[2] Chowdhury D., Self-organized patterns and traffic flow in colonies of organisms: from bacteria and social insects to vertebrates*, Phase Transitions* 77 601–624 (2004).

[3] Toner, J., Tu, Y. and Ramaswamy, S., Hydrodynamics and phases of flocks*, Annals of Physics* 318 170-244 (2005).

[4] Flierl G., Grünbaum D., Levins S. and Olson D., From Individuals to Aggregations: the Interplay between Behavior and Physics, *J. theor. Biol.* 196, 397-454 (1999).

[5] Vicsek T., Czirók A., Ben-Jacob E., Cohen I. and Shochet, O., Novel type of phase transition in a system of self-driven particles, *Phys. Rev. Lett.* 75 1226 (1995).

[6] Toner J. and Tu Y., Long-range order in a two-dimensional dynamical XY model: how birds fly together, *Phys. Rev. Lett.* 75 4326 (1995).

[7] Grégoire G., Chaté H. and Tu Y., Moving, and staying together without a leader, *Physica D* 181 157-170 (2003).

[8] Chaté H., Ginelli F. and Montagne, R., Simple Model for Active Nematics: Quasi-Long-Range Order and Giant Fluctuations, *Phys. Rev. Lett.* 96 180602 (2006).

[9] Narayan V., Menon N. and Ramaswamy S., Nonequilibrium steady states in a vibrated-rod monolayer: tetratic, nematic, and smectic correlations*, J. Stat. Mech.* P01005 (2006).

[10] Narayan V., Ramaswamy S. and Menon, N., Swarming Granular Nematic Long-Lived Giant Number Fluctuations in a Swarming Granular Nematic*, Science* 317 105-108 (2007).

[11] Galanis J., Harries D., Sackett D. L., Losert W. and Nossal R., Spontaneous Patterning of Confined Granular Rods, *Phys. Rev. Lett.* 96 028002 (2006).

[12] Aranson I. S., Volfson D. and Tsimring, L. S., Swirling motion in a system of vibrated elongated particles, *Phys. Rev. E* 75 051301 (2007).

[13] Blair D. L., Neicu T. and Kudrolli A., Vortices in vibrated granular rods*, Phys. Rev. E* 67 031303 (2003).

[14] Baskaran A. and Marchetti M. C., Enhanced Diffusion and Ordering of Self-Propelled Rods, *Phys. Rev. Lett*. 101 268101 (2008).

[15] Kudrolli A., Lumay G., Volfson D. and Tsimring L. S., Swarming and Swirling in Self-Propelled Polar Granular Rods, *Phys. Rev. Lett*. 100 058001 (2008).

[16] Vásárhelyi G., Ábel D., Tarcai N., Virágh Cs., Várkonyi P. L. and Vicsek T., Phases and phase transitions in the collective dynamics of simple robotic flocks. *Manuscript in preparation.*

[17] D'Orsogna M. R., Chuang Y. L., Bertozzi A. L. and Chayes, L. S., Self-Propelled Particles with Soft-Core Interactions: Patterns, Stability, and Collapse*, Phys. Rev. Lett*. 96 104302 (2006).

[18] Peruani F., Deutsch A. and Bär M., Nonequilibrium clustering of self-propelled rods, *Phys. Rev. E* 74 030904(R) (2006).

[19] Grossman D., Aranson I. S.and Ben Jacob E., Emergence of agent swarm migration and vortex formation through inelastic collisions, *New J. Phys.* 10 023036 (2008).

[20] Derzsi A., Szőllősi G. and Vicsek, T., unpublished.

[21] Deseigne J., Dauchot O., Chaté H., Collective Motion of Vibrated Polar Disks, *Phys. Rev. Lett.* 105 098001 (2010).

[22] Ahmadi A., Marchetti M. C.and Liverpool T. B., Hydrodynamics of isotropic and liquid crystalline active polymer solutions, *Phys. Rev. E* 74 061913 (2006).

[23] Kraikivski P., Lipowsky R., Kierfeld J., Enhanced ordering of interacting filaments by molecular motors, *Phys. Rev. Lett*. 96 258103 (2006).

[24] Ziebert F., Aranson I. S., Tsimring L. S., Effects of cross-links on motor-mediated filament organization, *New J. Phys.* 9 421 (2007)

[25] Riedel I. H., Kruse K. and Howard J., A Self-Organized Vortex Array of Hydrodynamically Entrained Sperm Cells, *Science* 309 300-303 (2008).

[26] Sokolov A., Aranson I. S., Kessler J. O. and Goldstein R. O., Concentration Dependence of the Collective Dynamics of Swimming Bacteria, *Phys. Rev. Lett.* 98 158102 (2007).

[27] Couzin I. D., Krause J., Franks N. R. and Levin S. A., Effective leadership and decision making in animal groups on the move, *Nature* 433 513-516 (2005).

[28] Nabet B., Leonard N. E., Couzin I. D., Levin S. A., Dynamics of Decision Making in Animal Group Motion, J. Nonlinear Sci. 19 399-435 (2009).

[29] N. Shimoyama N., Sugawara K., Mizuguchi T., Hayakawa Y., Sano M., Collective Motion in a System of Motile Elements, *Phys. Rev. Lett.* 76 3870-3873 (1996).

[30] M. Ballerini, et al., Interaction ruling animal collective behavior depends on topological rather than metric distance: Evidence from a field study, *Proc. Natl. Acad. Sci. USA* 105 1232-1237 (2008).

[31] Couzin I. D., Krause J., James R., Ruxton G. D., Franks N. R., Collective Memory and Spatial Sorting in Animal Groups, *J. Theor. Biol.* 218 1-11 (2002).

[32] Mikhailov A. S. , Zanette D. H., Noise-induced breakdown of coherent collective motion in swarms, *Phys. Rev. E* 60 4571-4575 (1999).

[33] Levine H., Rappel W-J., Cohen I., Self-organization in systems of self-propelled particles, *Phys. Rev. E* 63 017101 (2001) .

[34] Baruh H., *Analytical Dynamics*, WCB McGraw-Hill (1999).

[35] Animations illustrating the effect of model parameters π_3 and π_4, attached as Additional Material. The individuals' preference vectors ($\mathbf{p}_i$) are indicated by red lines. Animation 1 shows dynamics with original parameter values. In Animation 2, π_3 is modified to 0.1 (low turning rates). Individuals hardly exhibit any contact. In Animation 3, π_3=10 (high turning rates). Translational motion of the group is suppressed by social attraction. In Animation 4, π_4 is 1 instead of 10. Excentric contact forces hardly rotate particles. In Animation 5, π_4 is 100. Upon contact, particles rotate very easily. They form pairs moving shoulder to shoulder, whose steering response to social attraction is almost blocked by contact forces.

[36] Swaminathan S., Ziebert F., Aranson I. S., Karpeev D., Patterns and intrinsic fluctuations in semi-dilute motor-filament systems, *Europhys. Lett.* 90 28001 (2010).

[37] Zhou C., Kurths J., Noise-Induced Phase Synchronization and Synchronization Transitions in Chaotic Oscillators, *Phys. Rev. Lett.* 88 230602 (2002).

[38] Van den Broeck C., Parrondo J. M. R., Toral R., Noise-Induced Nonequilibrium Phase Transition, *Phys. Rev. Lett.* 73 3395 (1994).

[39] Two animations with 50 uninformed (π_2=0) individuals attached as Additional Material. Shape parameters are π_1=1 and 4, respectively. Notice that the center of the camera window follows the center of mass of the group.

[40] Kluyver J. C., A local probability problem, *Nederl. Akad. Wetensch. Proc.* 8 341-350 (1906).

[41] Strutt J. W. (Lord Rayleigh), The problem of the random walk, *Nature* 72 318 (1905).

[42] Redon S., Kheddar A. and Coquillart, S., Gauss' Least Constraints Principle and Rigid Body Simulations, *Proc. 2002 IEEE International Conference on Robotics & Automation, Washington DC* (2002).